Crystal structure of *Staphylococcus aureus* exfoliative toxin D-like protein: Structural basis for the high specificity of exfoliative toxins

Ricardo B. Mariutti [a], Tatiana A.C.B. Souza [b], Anwar Ullah [a], Icaro P. Caruso [a],
Fábio R. de Moraes [a], Leticia M. Zanphorlin [c], Natayme R. Tartaglia [d, e, f], Nubia Seyffert [d],
Vasco A. Azevedo [d], Yves Le Loir [e, f], Mário T. Murakami [g], Raghuvir K. Arni [a, *]

[a] Multi User Center for Biomolecular Innovation, Department of Physics, IBILCE/UNESP, São José do Rio Preto, SP, Brazil
[b] Carlos Chagas Institute, FIOCRUZ-PR, Curitiba, PR, Brazil
[c] Bioethanol Science and Technology Laboratory (CTBE), National Center for Research in Energy and Materials, Campinas, SP, 13083-970, Brazil
[d] Cellular and Molecular Genetics Laboratory, Institute of Biological Sciences, Federal University of Minas Gerais, Belo Horizonte, MG, 270-901, Brazil
[e] INRA, UMR1253 STLO, Science et Technologie du Lait et de l'œuf, F-35042 Rennes, France
[f] Agrocampus Ouest, UMR1253 STLO, F-35042 Rennes, France
[g] Brazilian Biosciences National Laboratory (LNBio), National Center for Research in Energy and Materials, Campinas, SP, 13083-970, Brazil

ARTICLE INFO

ABSTRACT

Exfoliative toxins are serine proteases secreted by *Staphylococcus aureus* that are associated with toxin-mediated staphylococcal syndromes. To date, four different serotypes of exfoliative toxins have been identified and 3 of them (ETA, ETB, and ETD) are linked to human infection. Among these toxins, only the ETD structure remained unknown, limiting our understanding of the structural determinants for the functional differentiation between these toxins. We recently identified an ETD-like protein associated to *S. aureus* strains involved in mild mastitis in sheep. The crystal structure of this ETD-like protein was determined at 1.95 Å resolution and the structural analysis provide insights into the oligomerization, stability and specificity and enabled a comprehensive structural comparison with ETA and ETB. Despite the highly conserved molecular architecture, significant differences in the composition of the loops and in both the N- and C-terminal α-helices seem to define ETD-like specificity. Molecular dynamics simulations indicate that these regions defining ET specificity present different degrees of flexibility and may undergo conformational changes upon substrate recognition and binding. DLS and AUC experiments indicated that the ETD-like is monomeric in solution whereas it is present as a dimer in the asymmetric unit indicating that oligomerization is not related to functional differentiation among these toxins. Differential scanning calorimetry and circular dichroism assays demonstrated an endothermic transition centered at 52 °C, and an exothermic aggregation in temperatures up to 64 °C. All these together provide insights about the mode of action of a toxin often secreted in syndromes that are not associated with either ETA or ETB.

© 2015 Elsevier Inc. All rights reserved.

1. Introduction

Staphylococcus aureus, the Gram-positive bacterial pathogen, triggers a wide spectrum of infection and is the primary causative agent of pyogenic infections which can result in septicemia, osteomyelitis and meningitis, is encountered in humans and approximately 35% of the population are carriers. It is also found in warm-blooded animals [1] and is a major causative agent of mastitis in ruminants, causing thus huge economic losses in the milk production [2].

S. aureus secretes different exfoliative toxins (ETs) that result in toxin-mediated staphylococcal syndromes. These disorders range from localized bullous impetigo to staphylococcal scalded skin syndrome (SSSS) in which superficial skin blistering and exfoliation follow widespread painful erythema [3]. Thus far, four different serotypes of exfoliative toxins ETA, ETB, ETC, and ETD have been identified [4] and three of them (ETA, ETB, and ETD) are related to human infection [5]. Some ET and ET-like proteins are also found associated to skin infections in animal hosts and show cleavage specificity against human or animal desmogleins [6].

SSSS and bullous impetigo, the major human exfoliative dermatitis caused by ETs [7], primarily affect newborns with exfoliation of 50% or more of the skin [8], are a result of the action of ETA and ETB [9]. On the other hand, ETD seems to be associated with the formation of cutaneous abscesses and furuncles [10], characterized by extensive tissue damage, which might be a result of the localized action of ETs [11].

ETA and ETB are atypical glutamic acid-specific trypsin-like serine proteinases and their accumulation in the skin causes disruption of desmosomes via proteolytic cleavage of desmoglein I [7,12]. ETD mediates intra-epidermal cleavage through the granular layer of the epidermis of neonatal mice and induces epidermal blisters in newborn mice [5]. The mechanisms underlying substrate recognition by these proteases suggest that ETs recognize their substrates *via* both the classic P1 site interactions and significant secondary interactions involving the tertiary structural features of desmoglein [11].

We recently identified an ET-like protein in *S. aureus* O46, a strain associated to mild ewe mastitis [13,14]. It showed high similarity with previously described *S. aureus* ETD in its amino acid primary sequence, including the presence of the typical catalytic site found in the other ET proteins described so far, and was thus named EDT-like. The exact role of this ETD-like variant in *S. aureus* colonization of the udder tissues or in the infection process in ruminant mastitis remains unknown.

The crystal structures of ETA and ETB [8,15–17] along with the structure of ETD-like presented here provide the structural basis for understanding the exquisite substrate specificity of these enzymes and their ability to only cleave a single bond in desmoglein 1 but not in other homologous desmogleins.

2. Materials and methods

2.1. Protein expression and purification

The gene corresponding to ETD-like was amplified from *S. aureus* O46 genomic DNA and cloned into a pD441 expression vector for further protein production and purification.

An isolated colony of *E. coli* C43 (DE3) *pLysS* transformed with pD441/ETD-like was grown for 16 h at 37 °C in LB medium supplemented with kanamycin (34 μg/mL). The culture grown overnight was diluted 100-fold with fresh LB broth containing kanamycin (34 μg/mL) and incubated at 30 °C until the optical density (OD_{600}) reached 0.5 and was subsequently induced with 0.2 mM IPTG for 16 h at 20 °C. The cells were collected by centrifugation at 2600 g for 10 min at 4 °C and suspended in a 20 mM Tris−HCl buffer pH 8.0 containing 500 mM NaCl, lysed by sonication and centrifuged at 15,000 g for 15 min. The supernatant was subjected to affinity chromatography using an immobilized nickel column (GE) under native conditions and further purified using a Superdex G75 10/300 GL column and the results were analyzed by SDS-PAGE.

2.2. Crystallization, data collection, processing and structure determination

Crystals were obtained by vapor diffusion when a protein concentration of 20 mg mL^{-1} in 100 mM HEPES Sodium pH 7.5 was equilibrated against a reservoir that additionally contained 30% 2-Propanol. Diffraction data were collected from a single flash frozen crystal in a 100 K gaseous nitrogen stream at the W01B-MX2 beamline at Brazilian Synchrotron Light Laboratory (LNLS, Campinas, Brazil). The wavelength of the radiation source was set to 1.458 Å and a Pilatus 2M detector was used to record the diffraction intensities. The crystal was exposed for 2 s per 0.1 degree of rotation

Table 1
Hydrodynamic and structural properties of ETD-like.

	DLS	AUC[a]
MW (kDa)	–	27.2
f/f_0	–	1.43
s (S)	–	2.2
Rs (nm)	2.8	–
Polydispersity (%)	30	–

[a] Calculated from sedimentation velocity data using SedFit software.

and a total of 1800 images collected. The data were indexed, integrated and scaled using the DENZO and SCALEPACK programs from the HKL-2000 package [18].

The structure was solved by molecular replacement using the atomic coordinates of ETB (PDB ID: 1DT2, 62% sequence identity) as a template and the program PHASER [19]. Model refinement was carried out using cycles of REFMAC5 [20] or phenix.refine [21] followed by visual inspection of the electron density maps and manual rebuilding with COOT [22]. Refinement cycles included secondary structure, reference-model restraints and translation/libration/screw parameters. The model quality was assessed using MolProbity [23]. Data collection and refinement statistics are presented in Table 1. The ETD-like atomic coordinates have been deposited with the RCSB Protein Data Bank under the accession code 5C2Z.

2.3. Hydrodynamic experiments

Sedimentation velocity experiments were carried out in an Optima XL-A analytical ultracentrifuge (Beckman) with the AN-60 Ti rotor set at 30,000 rpm at 15 °C. The ETD-like sedimentation data was monitored by absorbance at 230 nm and the experiments were performed with protein concentrations of 0.4 and 0.8 mg/mL prepared in 20 mM Hepes, 150 mM NaCl, pH 7.5. The SedFit software was used to process the AUC data [24] and the frictional ratio (f/f_0) was applied as a regularization parameter, which was allowed to drift freely. Buffer density (1.0039 g/mL) and viscosity (0.0102643 Poise), and the partial specific volume of the ETD-like (0.7346 mL/g) were estimated by the Sednterp program (http://www.jphilo.mailway.com/download.htm).

DLS measurements were performed using a ZETASIZER Nano series (Malvern Instruments) and the data acquisition was accomplished after the average of 14 runs at a constant temperature of 25 °C and protein concentration ranging from 1 mg/mL to 8 mg/mL in a 20 mM Hepes buffer pH 7.5 and 150 mM NaCl. The Zetasizer software was used to obtain the hydrodynamic radius (Rh) of ETD-like from the extrapolation of the translational diffusion coefficient (Dt) according to the Stokes−Einstein equation.

2.4. Differential scanning calorimetry (DSC)

DSC experiments were performed using N-DSC III (TA Instruments, USA) in the temperature ranges of 20−64 and 20−90 °C with a heating and cooling scan rate of 1 °C/min. The protein was diluted in a phosphate buffer (10 mM NaH_2PO_4, 100 mM NaF, pH 7.4) to a final concentration of 0.64 mg/mL. Both the calorimeter cells were loaded with the buffer solution, equilibrated at 20 °C for 10 min and scanned repeatedly as described above until the baseline was stable and reproducible. The sample cell was subsequently loaded with ETD-like and scanned in the same way. The baseline correction was conducted by subtracting the 'buffer vs. buffer' scan from the corresponding 'protein vs. buffer' scan and all measurements were repeated twice.

2.5. Circular dichroism spectroscopy

Circular dichroism spectroscopy was performed on a Jasco J-815 spectropolarimeter (Jasco, USA) with a Peltier-type temperature control system. The far UV–CD spectrum of ETD-like was collected from 260 to 190 nm at 20 °C in a 0.1 cm quartz cuvette. A scan speed of 50 nm/min was used with a response time of 1.0 s, spectral bandwidth of 1.0 nm and spectral resolution of 0.1 nm. The signal was averaged over 10 scans. Each spectrum was acquired independently twice. The protein was diluted to 7.35 μM in a phosphate buffer (5 mM NaH_2PO_4, 50 mM NaF, pH 7.4). In the thermal unfolding experiment, the protein sample was heated from 20 to 64 °C at a rate of 1.0 °C/min and ellipticity measurements were performed around the minimum of the ETD-like spectra (at 205 and 208 nm) every 2.0 °C. The contribution of the buffer was subtracted from the protein spectra. Percentages of secondary structure of ETD-like in solution were calculated with the CONTINLL software of the CDPro package, using the reference set of proteins SMP50 [25].

2.6. Molecular dynamics

Crystal structures from ETA and ETB were retrieved from the PDB (IDs: 1DUA and 1DT2, respectively). In order to compare the dynamical behavior of the three exfoliative proteins, 40 ns (4 × 10 ns) molecular dynamics simulations were performed using GROMACS 4.5.5 [26,27]. In each run, the protein was centered in a cubic box with edges of 1.0 nm away from any protein atom. The SPC/E water model was used and 0.1 M salt ions were added to the system in order to make it neutral. Energy minimizations were carried out with steepest descent integrator and conjugate gradient algorithm, using 1000 kJ mol^{-1} nm^{-1} as maximum force criterion. The particle mesh Ewald (PME) method for long-range electrostatic interaction [28] was used. In all simulations, a velocity rescaling thermostat [29] with a time constant of 0.1 ps was used to set the temperature to 300 K. The pressure of 1 atm was achieved by a Berendsen thermostat [30] with a time constant of 2 ps. Parallel linear constraint solver (LINCS) [31] was used to constrain all bonds. The systems were subject to 100 ps of NVT and NPT equilibration, using position constraints. Molecular dynamics simulations were carried out by 4 independent 10 ns runs with no position constraint, whatsoever. Following dynamics, the trajectories were concatenated and analyzed by different parameters, such as hydrogen bond pattern, potential energy profile, solvent area accessibility, residue mean fluctuation. Also, principal component analysis (PCA) using the *g_covar* and *g_anaeig* functions in GROMACS. The 10 first principal components (lowest frequencies) were used for comparison among the ETA, ETB and ETD-like.

3. Results and discussion

3.1. Thermodynamics and in solution behavior of ETD-like protein

The thermogram of purified ETD-like presented in Fig. 1A represents a typical protein unfolding process in the temperature range of 30–64 °C with an endothermic transition centered at 52 °C, and an exothermic aggregation in temperatures up to 64 °C. Inspection of the sample after completion of the heating and cooling scans indicated trace amounts of precipitated protein. It is likely that the observed exothermic behavior up to 64 °C is a result of protein aggregation. To confirm the thermal reversibility of ETD-like, a sample was heated to 64 °C and then cooled at the same scan rate (1 °C/min). The cooling scan of this sample indicated no transitions in the thermogram. These results indicate that the thermal unfolding of ETD-like is an irreversible process.

The CD spectrum of ETD-like presents structural characteristics of a structured protein since its minimum is located at 205 nm and the positive ellipticity is at 190 nm (Fig. 1B). The percentages of secondary structure were calculated using the CONTINLL program [25] and are in agreement with the crystallographic structure. Fig. 1C presents the temperature dependence of the average value of the ellipticity between 205 and 208 nm for the thermal unfolding of ETD-like. The melting temperature obtained by the CD measurements was 55 °C which is similar to the temperature determined by DSC, indicating significant correlation between the techniques.

Thermal denaturation studies of ETA and ETB using fluorescence spectroscopy indicated that these proteins present melting temperatures in the 57–59 and 52–54 °C ranges [32], which is very similar to the melting temperature of ETD-like (52–55 °C) determined in this work. The thermal unfolding process of ETD is similar to that of ETB, not only because of the greater similarity between the melting temperatures, but also due to the aggregation behavior that both present [33]. This may be due to the high sequence similarity of 54% between ETD-like and ETB. Secondary structure studies performed by CD spectroscopy also demonstrated that ETA and ETB present a higher percentage of β-sheet in solution [33], which is in agreement with the results obtained for ETD-like.

Hydrodynamic behavior of ETD-like was investigated by DLS (Table 1) and AUC (Table 1) experiments. The results indicate that the protein is monomeric in solution, since DLS estimates the protein hydrodynamic radius as 2.8 nm and AUC estimates the molecular mass as 27 kDa (Table 1). No evidence for oligomeric behavior of ETs is available, although some ET structures contain two molecules in the crystallographic asymmetric unit.
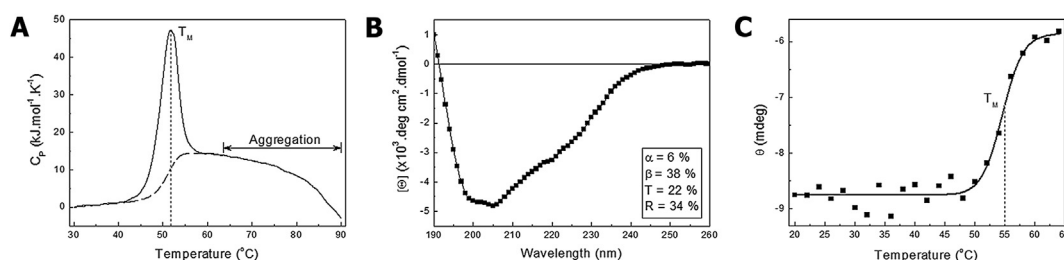

Fig. 1. Biophysical characterization of ETD-like. **(A)** DSC thermogram of ETD-like. Apparent excess heat capacity curve was recorded for ETD-like (0.64 mg/mL) in phosphate buffer (10 mM NaH_2PO_4, 100 mM NaF, pH 7.4) at a scan rate of 1 °C/min. The dotted line (- - -) indicates the melting temperature (T_M) and the dashed line (— —) represents the baseline used to correct the protein thermogram, excluding the temperature range in which the exothermic aggregation occurs. **(B)** Far UV–CD spectrum of ETD-like (7.35 μM) in phosphate buffer (5 mM NaH_2PO_4, 50 NaF, pH 7.4) at 20 °C. The letters α, β, T and R correspond to the percentage of α-helice, β-sheet, turn and random coil, respectively, calculated by the CONTINLL program. **(C)** Temperature dependence of average value of the ellipticity between 205 and 208 nm for the thermal unfolding of ETD-like obtained with scan rate of 1 °C/min. The solid line represents a sigmoidal fit and the dotted line indicates the melting temperature (T_M).

Table 2
Data collection and refinement statistics.

	ETD-like
Data collection	
Space group	$P2_1$
Cell dimensions	
a, b, c (Å)	49.41, 93.14, 50.48
β (°)	91.2
Molecules per AU[a]	2
Resolution range (Å)	50.47−1.95(2.0−1.95)
R_{meas} (%)	80.4(99.2)
$I/\sigma I$	9.43 (2.15)
CC(1/2)*	0.98 (0.62)
Completeness (%)	96.0 (86.0)
Multiplicity	6.9 (5.1)
Refinement	
Resolution (Å)	35.68−1.95 (2.0−1.95)
No. reflections	31,781
R_{work}/R_{free}	0.17/0.25
No. atoms	
Protein	4215
Mean B-factors (Å^2)	
Protein	25.79
R.m.s. deviations	
Bond lengths (Å)	0.007
Bond angles (°)	1.071
Ramachandran Plot	
Favored (%)	94.7
Allowed (%)	5.07
Disallowed (%)	0.2

Values in parentheses are for the highest-resolution shell.
*Correlation coefficient.
[a] AU, asymmetric unit.

3.2. The crystallographic structure of ETD-like

Four structures of ETA (PDB IDs: 1EXF, 1DUA, 1DUE and 1AGJ) and two structures of ETB (PDB IDs: 1DT2 and 1QTF) have been determined and with the structural data of ETD-like we can now understand their selectivity and modes of action.

The structure of ETD-like was determined and refined at 1.95 Å resolution and resulted in a crystallographic residual of 17.7% (R_{free} 25.3%) (Table 2). The high structural similarity between exfoliative toxins ETA, ETB and ETD-like protein, which share about 50% sequence identity, is evidenced by the low RMSD values of the superposed structures (ETA−ETB: 1.27 Å, ETA−ETD-like: 1.43 Å and ETB−ETD-like: 1.00 Å). The following structural characteristics are shared between the ETs from S. aureus: (i) protein fold is characterized by two six-strand β-barrels whose axes lie roughly perpendicular to each other as in other trypsin-like serine proteases, (ii) the Greek key motif consists of four adjacent antiparallel strands and their linking loops, (iii) the N- and C-terminal α-helical extensions and (iv) the active site is located at the interface of the two barrels that includes an aspartic acid, a histidine, and the catalytic serine residue (Fig. 2A).

The distinct size (ETD-like, ETA, ETB are composed of 249, 242 and 246 residues, respectively) and pI values (pI$_{ETD-like}$ = 7.8 [34], pI$_{ETA}$ = 7.0 and pI$_{ETB}$ = 6.95 [35]) indicate that despite the high structural conservation, structural differences associated with each ET may account for the observed functional differences. Detailed sequence and structural analyses permitted the identification of regions specific for each ET (Figs. 2 and 3, and Table 3) and are described below.

3.3. Sequence and conformation of loops related to substrate binding and specificity

Loops A, B, C and D are considered the determinants for subsite preferences in these proteins [17,35,36]. Distinct conformations of loops B and D are observed between ETA and ETD-like (Fig. 2B). In ETB, structural differences between loops A and B are observed when this structure is superposed with ETD-like (Fig. 2C). Sequence
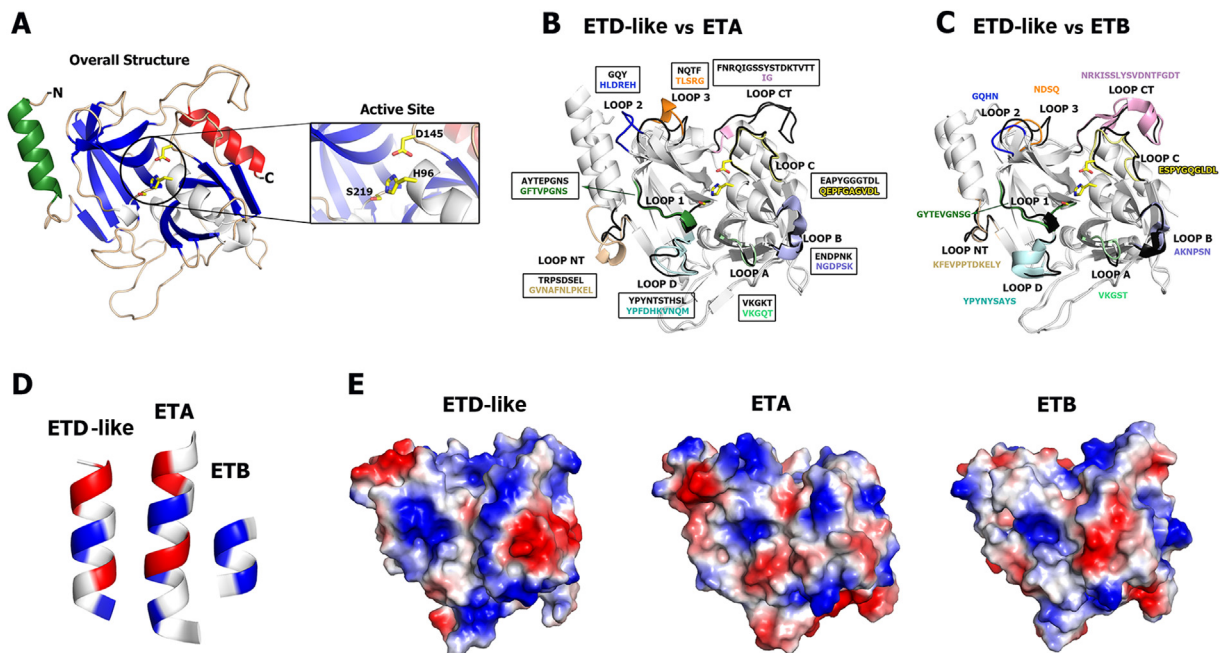

Fig. 2. Structural analysis of ETD-like. **(A)** Overall ETD-like structure. The enzyme is folded into two six-strand β-barrels (blue) whose axes that are roughly perpendicular as other trypsin-like serine proteases. The N- and C-terminal α-helices are colored in green and red, respectively. The active site of the molecule is amplified to identity the three catalytic residues. **(B and C)** Analysis of loops involved in the selectivity between ETD-like (this work), ETA (PDB ID: 1EXF) and ETB (PDB ID: 1DT2). The loops in ETD-like are colored in black and, in ETA and ETB, they are colored according to each loop. **(D)** Positive (blue) and negative (red) residues comprising the N-terminal α-helix of ETD-like, ETA and ETA. (D) Surface charge distribution around the catalytic interface of ETD-like, ETA and ETB. (For interpretation of the references to color in this figure legend, the reader is referred to the web version of this article.)
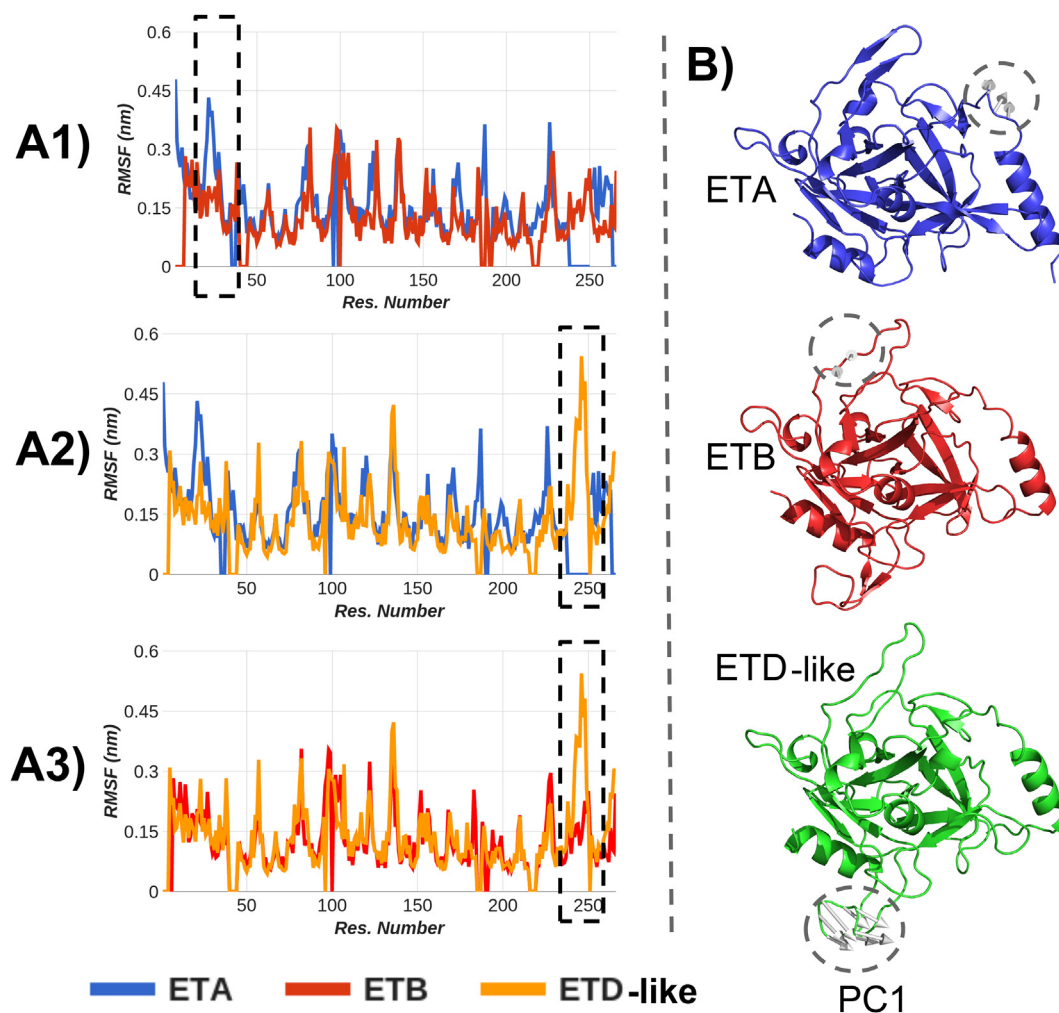
Fig. 3. Molecular dynamics simulations and structural comparisons between ETD-like, ETA and ETB. (A) Comparison of Root Mean Square Fluctuation for each amino acid residue. ETA's N-terminal is more flexible as compared to ETB and ETD-like. ETD-like C-Terminal region, absent from ETA, is more flexible as compared to ETB. (B) Projection of the molecular dynamics trajectories onto the first principal component highlighting regions found to be more flexible among ETA, ETB and ETD-like.

Table 3
Primary sequence analysis of ETs.

	ETD-like amino-acid residues
ETD-like amino-acid residues conserved with ETA	56, 57, 58, 91, 97, 104, 107, 108, 115, 119, 128, 155, 216, 231
ETD-like amino-acid residues conserved with ETB	37, 38, 39, 41, 46, 50, 52, 59, 64, 65, 69, 70, 72, 99, 109, 111, 116, 130, 132, 133, 137, 140, 148, 150, 154, 160, 163, 170, 171, 176, 177, 182, 188, 189, 191, 194, 195, 196, 199, 203, 204, 209, 211, 215, 226, 236, 238, 239, 240, 243, 244, 246, 249, 250, 251, 253, 255, 257, 258, 260, 265, 266, 269, 270, 271, 274, 275.
Amino-acid residues exclusive for ETD-like	40, 42−45, 47−49, 50, 53, 60, 62,63,68,78, 80, 84, 91, 95, 100, 102, 103, 106, 113, 114, 118, 120−125, 127, 131, 136, 138, 142, 144, 147, 156, 157, 164, 165, 168, 172, 173, 175, 181, 190, 192, 193, 197, 202, 205, 206, 207, 208, 212, 227, 241, 242, 245, 247, 248, 252, 254, 256, 259, 261, 263, 264, 267, 268, 276, 277, 278, 279.

comparisons indicate that the loop B is the most variable, whereas loops A, C and D present a fair degree of conservation (Fig. 2).

Loops 1, 2, and 3 are important in determining the specificity of the S1 subsite [17,36,37], and loop 2 is considered to be important for the proper positioning of the substrate in the active site of serine proteases, as residues along the loop form hydrogen bonds with the substrate [37]. Loop 1 is fully conserved in ETA, ETB and ETD-like (Fig. 2B,C). Conformational changes are observed in loops 2 and 3 of ETD-like when compared with the corresponding regions in ETA (Fig. 2B). The sequences in these loops are not

conserved between the ETs (Fig. 2B,C). When the ETD-like and ETB structures are compared, sequence and structural differences are principally observed in loop 3 and thus likely play a role in determining P1 specificity (Fig. 2C).

3.4. Loops connected to the N- and C-terminal α-helices are characteristic for each ET

Amino acids in the loops A−D and 1−3 participate in the interactions with the substrate; however, variations are also observed

in other loops of the ETD-like structure, which do not have defined roles in recognition or specificity. These differences reside in the loop connecting the N-terminal α-helix and the β1strand of ETD-like in relation to ETA (referred to as loop NT) and in the loop in the proximal region of the C-terminal α-helix (referred to as loop CT), which is also quite different in these two toxins (Fig. 2B,C). These regions differ both in composition and conformation and are considered the most flexible zones in these toxins, which might be associated with conformational changes upon substrate binding. In comparison to ETA, ETD-like has a very long loop CT inducing a different orientation of the C-terminal helix (Fig. 2B). In relation to ETB, these two loops are relatively similar in length and composition, indicating that these regions seem to be involved in the functional differentiation between ETD-like and ETA, and not to ETB. Molecular dynamics simulations indicate that the ETA loop NT is found to be more flexible than in ETB and ETD-like. This region is more conserved between ETB and ETD-like but not in ETA. This region in ETA is an extension of the N-terminal α-helix (α1), and in both ETB and ETD-like this helix is considerable shorter and the loop connecting the C-terminal helix, is more flexible in ETD-like than in ETB (Fig. 3).

3.5. N-terminal α-helix of ETs presents differential charge profile and forms distinct interactions

Structural differences are not restricted to the interfacial loops in the ETs structures; the N-terminal α-helix is highly charged in ETA, ETB and ETD-like, but the charge profile is significantly different, principally between ETD-like/ETA and ETB (Fig. 2D). The electrostatic potential at these helices indicates that the interactions formed by the residues from the N-terminal region are also different. The first residues of ETD-like (Met[1]–Glu[3], ETD-like numbering) are in contact with residues of loop 3, which differ from those of ETA whose N-terminal residues are in contact with loop 2. In ETB, Tyr[3] (ETB numbering) forms part of a buried hydrophobic interface with residues Phe[172], Phe[178] and Leu[210] (ETB numbering) of the C-terminal barrel domain as well as Ile[8], Leu[11], and Phe[15] (ETB numbering) of the N-terminal helix. Although the triad position of Phe[172], Phe[178] and Leu[210] (ETB numbering) is preserved in ETD-like, interactions formed by these residues are not the same. In ETD-like, the corresponding residues for Ile[8] and Leu[11] (ETB numbering) are Asp[36] and Ile[39] (ETD-like numbering).

3.6. Dynamics of ETA, ETB and ETD-like

To further compare the dynamics of the three toxins, projection of the 40 ns trajectories onto the two first principal components reveal that the intrinsic dynamics of ETA, ETB and ETD-like differ as presented in Fig. 3. The ETA dynamics indicate that the N-terminal helix and the loop comprising the segment K[75]–K[83] (ETA numbering) are the most mobile regions (Fig. 3). On the other hand, ETB is highly flexible in the loop consisting of Q[82]–T[93] (ETB numbering). In this loop, ETA has a β-strand that is not present in either ETB or ETD-like and displays low sequence identity with ETA. The ETD-like C-terminal loop is more flexible when compared to ETB. This is mainly due to G[254] in the position of S[220] in ETB. Also, the K[261] in ETD-like replaces D[226] from ETB. This negative to positive charge inversion coupled to the higher mobility of this loop in ETD-like might influence substrate recognition.

These structural deviations may influence the protein-substrate interactions. ETA, ETB and ETD are able to hydrolyze Dsg-1 both in vitro and in vivo [7,12,38,39] with hydrolysis being highly dependent on the conformation of Dsg-1 [40] and calcium ions [40–42] with cleavage occurring at exactly the same site [12]. Although, the substrate is common to all ETs, human-infecting

strains of S. aureus produce mainly ETA and ETB, and ETD is less frequently encountered than the other two toxins [5,43]. ETD-producing strains are mainly isolated from furuncles or cutaneous abscesses and not from the same tissues as the two other toxins [5,10]. The differences identified at the structural level here might also somehow reflect an adaptation to ruminant hosts.

In conclusion, the elucidation of the crystal structure of this ETD-like protein enables detailed structural comparisons of ETD-like with ETA and ETB and is important for the identification of specific features associated with the ETs from S. aureus of various host origins.

References

[1] V. Peton, Y. Le Loir, Staphylococcus aureus in veterinary medicine, Infect. Genet. Evol. 21 (2014) 602–615.

[2] C. Le Maréchal, E. Vautor, Y. Le Loir, Mastites impact on technological properties of milk and quality of milk products, Dairy Sci. Technol. 91 (2011) 247–282.

[3] P. Benson, Dermatologic manifestations of staphylococcal scalded skin syndrome, Medscape. http://emedicine.medscape.com/article/1053325-overview.

[4] G. Prevost, P. Couppie, H. Monteil, Staphylococcal epidermolysins, Curr. Opin. Infect. Dis. 16 (2003) 71–76.

[5] T. Yamaguchi, K. Nishifuji, M. Sasaki, Y. Fudaba, M. Aepfelbacher, T. Takata, M. Ohara, H. Komatsuzawa, M. Amagai, M. Sugai, Identification of the Staphylococcus aureus etd pathogenicity island which encodes a novel exfoliative toxin, ETD, and EDIN-B, Infect. Immun. 70 (2002) 5835–5845.

[6] K. Nishifuji, M. Sugai, M. Amagai, Staphylococcal exfoliative toxins: "Molecular scissors" of bacteria that attack the cutaneous defense barrier in mammals, J. Dermatol. Sci. 49 (2008) 2131.

[7] M. Amagai, N. Matsuyoshi, Z.H. Wang, C. Andl, J.R. Stanley, Toxin in bullous impetigo and staphylococcal scalded-skin syndrome targets desmoglein 1, Nat. Med. 6 (2000) 1275–1277.

[8] G.M. Vath, C.A. Earhart, D.D. Monie, J.J. Iandolo, P.M. Schlievert, D.H. Ohlendorf, The crystal structure of exfoliative toxin b: a superantigen with enzymatic activity, Biochemistry 38 (1999) 10239–10246.

[9] O. Yamasaki, T. Yamaguchi, M. Sugai, C. Chapuis-Cellier, F. Arnaud, F. Vandenesch, J. Etienne, G. Lina, Clinical manifestations of staphylococcal scalded-skin syndrome depend on serotypes of exfoliative toxins, J. Clin. Microbiol. 43 (2005) 1890–1893.

[10] O. Yamasaki, A. Tristan, T. Yamaguchi, M. Sugai, G. Lina, M. Bes, F. Vandenesch, J. Etienne, Distribution of the exfoliative toxin D gene in clinical Staphylococcus aureus isolates in France, Clin. Microbiol. Infect. 12 (2006) 576–596.

[11] M. Bukowski, B. Wladyka, G. Dubin, Exfoliative toxins of Staphylococcus aureus, Toxins (Basel) 2 (2010) 1148–1165.

[12] Y. Hanakawa, N.M. Schechter, C. Lin, L. Garza, H. Li, T. Yamaguchi, Y. Fudaba, K. Nishifuji, M. Sugai, M. Amagai, J.R. Stanley, Molecular mechanisms of blister formation in bullous impetigo and staphylococcal scalded skin syndrome, J. Clin. Investig. 110 (2002) 53–60.

[13] C. Le Maréchal, J. Jardin, G. Jan, S. Even, C. Pulido, J.M. Guibert, D. Hernandez, P. François, J. Schrenzel, D. Demon, E. Meyer, N. Berkova, R. Thiéry, E. Vautor, Y. Le Loir, Staphylococcus aureus seroproteomes discriminate ruminant isolates causing mild or severe mastitis, Vet. Res. 42 (2011) 35–55.

[14] C. Le Maréchal, N. Seyffert, J. Jardin, D. Hernandez, G. Jan, L. Rault, V. Azevedo, P. François, J. Schrenzel, M. van de Guchte, S. Even, N. Berkova, R. Thiéry, J.R. Fitzgerald, E. Vautor, Y. Le Loir, Molecular basis of virulence in Staphylococcus aureus mastitis, PLoS ONE 6 (2011) 27354.

[15] J. Cavarelli, G. Prevost, W. Bourguet, L. Moulinier, B. Chevrier, B. Delagoutte, A. Bilwes, L. Mourey, S. Rifai, Y. Piemont, D. Moras, The structure of Staphylococcus aureus epidermolytic toxin A, an atypic serine protease, at 1.7 Å resolution, Structure 5 (1997) 813–824.

[16] G.M. Vath, C.A. Earhart, J.V. Rago, M.H. Kim, G.A. Bohach, P.M. Schlievert, D.H. Ohlendorf, The structure of the superantigen exfoliative toxin A suggests a novel regulation as a serine protease, Biochemistry 36 (1997) pp.1559–pp.1566.

[17] A.C. Papageorgiou, L.R.W. Plano, C.M. Collins, K.R. Acharya, Structural similarities and differences in Staphylococcus aureus exfoliative toxins A and B as revealed by their crystal structures, Protein Sci. 9 (2000) 610–618.

[18] Z. Otwinowski, W. Minor, Processing of X-ray diffraction data collected in oscillation mode, in: C.W. Carter, R.M. Sweet (Eds.), Methods in Enzymology: Macromolecular Crystallography, Part a, vol. 276, Academic Press, New York, USA, 1997, pp. 307–326.

[19] A.J. McCoy, R.W. Grosse-Kunstleve, P.D. Adams, M.D. Winn, L.C. Storoni, R.J. Read, Phaser crystallographic software, J. Appl. Crystallogr. 40 (2007) 658–674.

[20] G.N. Murshudov, A.A. Vagin, E.J. Dodson, Refinement of macromolecular structures by the maximum-likelihood method, Acta Crystallogr. D Biol. Crystallogr. 53 (1997) 240–255.

[21] P.V. Afonine, R.W. Grosse-Kunstleve, N. Echols, J.J. Headd, N.W. Moriarty,

M. Mustyakimov, T.C. Terwilliger, A. Urzhumtsev, P.H. Zwart, P.D. Adams, Towards automated crystallographic structure refinement with phenix.refine, Acta Crystallogr. D Biol. Crystallogr. 68 (2012) 352—367.

[22] P. Emsley, K. Cowtan, Coot: model-building tools for molecular graphics, Acta Crystallogr. D Biol. Crystallogr. 60 (2004) 2126—2132.

[23] V.B. Chen, W.B. Arendall, J.J. Headd, D.A. Keedy, R.M. Immormino, G.J. Kapral, L.W. Murray, J.S. Richardson, D.C. Richardson, MolProbity: all-atom structure validation for macromolecular crystallography, Acta Crystallogr. D Biol. Crystallogr. 66 (2010) 12—21.

[24] J.C. Borges, C.H.I. Ramos, Analysis of molecular targets of mycobacterium tuberculosis by analytical ultracentrifugation, Curr. Med. Chem. 18 (2011) 1276—1285.

[25] N. Sreerama, R.W. Woody, A self-consistent method for the analysis of protein secondary structure from circular dichroism, Anal. Biochem. 282 (2000) 252—260.

[26] D. van der Spoel, E. Lindahl, B. Hess, G. Groenhof, A.E. Mark, H.J.C. Berendsen, GROMACS: fast, flexible and free, J. Compt. Chem. 26 (2005) 1701—1719.

[27] B. Hess, C. Kutzner, D. van der Spoel, E. Lindahl, GROMACS 4: algorithms for highly efficient, load-balanced, and scalable molecular simulation, J. Chem. Theory Comput. 4 (2008) 435—447.

[28] U. Essmann, L. Perera, M.L. Berkowitz, T. Darden, H. Lee, L.G. Pedersen, A smooth particle mesh Ewald method, J. Chem. Phys. 103 (1995) 8577—8592.

[29] G. Bussi, D. Donadio, M. Parrinello, Canonical sampling through velocity rescaling, J. Chem. Phys. 126 (2007) 014101.

[30] H.J.C. Berendsen, J.R. Grigera, T.P. Straatsma, The missing term in effective pair potentials, J. Phys. Chem. 91 (1987) 6269—6271.

[31] B. Hess, P-LINCS: a parallel linear constraint solver for molecular simulation, J. Chem. Theory Comput. 4 (2008) 116—122.

[32] Y. Piémont, E. Piémont, D. Gérard, Fluorescence studies stability of staphylococcal exfoliative toxins A and B, FEMS Microbiol. Lett. 36 (1986) 245—249.

[33] C.J. Bailey, S.R. Martin, P.M. Bayley, A circular-dichroism study of epidermolytic toxins A and B from *Staphylococcus aureus*, Biochem. J. 203 (1982)

[34] E. Gasteiger, C. Hoogland, A. Gattiker, S. Duvaud, M.R. Wilkins, R.D. Appel, A. Bairoch, Protein identification and analysis tools on the ExPASy server, in: J.M. Walker (Ed.), The Proteomics Protocols Handbook, Humana Press, Totowa, USA, 2005, pp. 571—607.

[35] J.C. De Azavedo, C.J. Bailey, J.P. Arbuthnott, Assays for epidermolytic toxin of *Staphylococcus aureus*, Methods. Enzymol. 165 (1988) 32—36.

[36] I. Schechter, A. Berger, On the size of the active site in proteases I. Papain, Biochem. Biophys. Res. Commun. 27 (1968) 157—162.

[37] J.J. Perona, C.S. Craik, Structural basis of substrate specificity in the serine proteases, Protein Sci. 4 (1995) 337—360.

[38] M. Amagai, T. Yamaguchi, Y. Hanakawa, K. Nishifuji, M. Sugai, J.R. Stanley, Staphylococcal exfoliative toxin B specifically cleaves desmoglein 1, J. Investig. Dermatol. 118 (2002) 845—850.

[39] Y. Yamaguchi, K. Takahashi, B.Z. Zmudzka, A. Kornhauser, S.A. Miller, T. Tadokoro, Human skin responses to UV radiation: pigment in the upper epidermis protects against DNA damage in the lower epidermis and facilitates apoptosis, FASEB J. 20 (2006) 1486—1488.

[40] Y. Hanakawa, T. Selwood, D. Woo, C. Lin, N.M. Schechter, J.R. Stanley, Calcium-dependent conformation of desmoglein 1 is required for its cleavage by exfoliative toxin, J. Investig. Dermatol. 121 (2003) 383—389.

[41] Y. Hanakawa, N.M. Schechter, C. Lin, K. Nishifuji, M. Amagai, J.R. Stanley, Enzymatic and molecular characteristics of the efficiency and specificity of exfoliative toxin cleavage of desmoglein 1, J. Biol. Chem. 279 (2004) 5268—5277.

[42] S. Getsios, A.C. Huen, K.J. Green, Working out the strength and flexibility of desmosomes, Nat. Rev. Mol. Cell Biol. 5 (2004) 271—281.

[43] K. Becker, A.W. Friedrich, G. Lubritz, M. Weilert, G. Peters, C. Von Eiff, Prevalence of genes encoding pyrogenic toxin superantigens and exfoliative toxins among strains of *Staphylococcus aureus* isolated from blood and nasal specimens, J. Clin. Microbiol. 41 (2003) 1434—1439.

pp.775—pp.778.